CHEMISTRY OF MATERIALS
Article

Chem. Mater. **2009,** *21,* 5187–5195 5187
DOI:10.1021/cm902073g

Phase-Tunable Fabrication of Consolidated (α+β)-TiZr Alloys for Biomedical Applications through Molten Salt Electrolysis of Solid Oxides

Junjun Peng,[†] Hualin Chen,[†] Xianbo Jin,*[,†] Tao Wang,[†] Dihua Wang,[†] and George Z. Chen*[,†,‡]

[†]*College of Chemistry and Molecular Sciences, Hubei Key Laboratory of Electrochemical Power Sources, Wuhan University, Wuhan,430072, People's Republic of China, and* [‡]*Department of Chemical and Environmental Engineering, Faculty of Engineering, The University of Nottingham, Nottingham, NG7 2RD, United Kingdom*

Received July 9, 2009. Revised Manuscript Received September 12, 2009

Electrochemical reduction of a solid TiO_2-ZrO_2 mixture (molar ratio = 1:1) to the TiZr alloys in a consolidated porous structure was studied by constant cell voltage electrolysis in molten $CaCl_2$ at 900 °C. For the first time, and surprisingly, it was found that tuning the α- and β-phases in the TiZr alloys could be easily realized by controlling the electrolysis time or, specifically, the oxygen content in the alloys. Oxygen acted as a phase-transition inhibitor from the high-temperature β-TiZr to the low-temperature α-TiZr, leading to metastable β-TiZr or (α+β)-TiZr as the product at room temperature. However, if the oxygen content decreased to <1100 ppm, only α-TiZr was collected, even when the electrolytic alloy was directly quenched in water. The consolidated porous (α+β)-TiZr alloys possessed elastic moduli in the range of 20−40 GPa, matching closely to that of natural bone (10−30 GPa). They also exhibited excellent corrosion resistance in the Ringer solution. These novel findings promise a simple, one-step, low-energy, and environmentally friendly electrochemical process for the production of β-phase containing TiZr alloys as medical implant materials without any added expensive and/or bio-incompatible elements.

1. Introduction

Titanium and its alloys possess many outstanding merits for materials uses, such as high strength-to-weight ratios, excellent mechanical properties, and corrosion resistance. In the past several decades, titanium and its alloys have become the preferred artificial bone implant materials, because of their better biocompatibility and relatively smaller elastic modulus (∼100 GPa), compared to stainless steels and CoCrMo alloys. However, there is still a great mismatch of elastic modulus between the titanium-based implants and natural bone (10−30 GPa), which together with the weak wear resistance of the implants, are currently identified as the major reasons for the bone resorption and loosening of the implant in host bodies.[1−6]

It has been proven that introducing the β-phase into the α-phase titanium alloys is a potential way to reduce the elastic modulus and enhance the strength, as well as improve the wear resistance and corrosion resistance of the surgical implantation. Such changes may be realized by controlling the elemental composition of the alloys, and/or through thermomechanical processing.[1−8] Some elements, which are termed "β-stabilizers" (such as vanadium, molybdenum, iron, tungsten, chromium, and nickel), can help to form a β-phase or metastable β-phase in titanium alloys. However, for orthopedic applications, most of these β-stabilizers should be avoided, because they will cause rejection or release metal ions in the physiological environment.[1−6]

Both titanium and zirconium are fully biocompatible, and their alloys, as reported in the literature, showed enhanced strength relative to pure titanium.[9−11] Furthermore, the ZrO_2 in the surface oxide layer could strengthen the wear resistance of the implant.[4] However, the Ti−Zr binary alloys are usually present in the α-phase, and their high intrinsic elastic moduli (∼100−120 GPa) must be reduced before surgical practices, which empirically would be achieved by alloying with the β-stabilizers.[4−8] For this purpose, only some expensive elements (such as niobium and tantalum) would be recommended, considering that biocompatibility is primary; however, they are

*Authors to whom correspondence should be addressed. Tel.: +86 27 68756319 (X.B.J.), +44 (0)115 9514171 (G.Z.C.); Fax: +86 27 68756319 (X.B.J.), +44 (0)115 9514115 (G.Z.C.); E-mail: xbjin@whu.edu.cn (X.B.J.), george.chen@nottingham.ac.uk (G.Z.C.).

(1) Leyens, C.; Peters, M. *Titanium and Titanium Alloys: Fundamentals and Applications*; Wiley−VCH: Weinheim, Germany, 2003.
(2) Yang, H.W.; Lin, C. *Metall. Mater. Trans. A* **2006**, *37*, 3191.
(3) Berteaux, O.; Popoff, F.; Thomas, M. *Metall. Mater. Trans. A* **2008**, *39*, 2281.
(4) Long, M.; Rack, H. J. *Biomaterials* **1998**, *19*, 1621.
(5) Niinomi, M. *Metall. Mater. Trans. A* **2002**, *33*, 477.
(6) He, G.; Hagiwara, M. *Mater. Sci. Eng. C* **2006**, *26*, 14.
(7) Qazi, J. I.; Marquardt, B.; Rack, H. J. *JOM* **2004**, *56*, 49.
(8) Liu, Z.; Welsch, G. *Metall. Trans. A* **1988**, *19A*, 527.
(9) Ho, W. F.; Chen, W. K.; Wu, S. C.; Hsu, H. C. *J. Mater. Sci.: Mater. Med.* **2008**, *19*, 3179.
(10) Ikarashi, Y.; Toyoda, K.; Kobayashi, E. J. *Jpn. Inst. Met.* **2007**, *71*, 395.
(11) Wen, C. E.; Yamada, Y.; Hodgson, P. D. *Mater. Sci. Eng. C* **2006**, *26*, 1439.

Published on Web 10/19/2009

not welcomed in terms of cost. It has also been suggested that the construction of a proper porous structure can reduce the apparent elastic modulus of the implant, although with some sacrifice of the strength.[11,12]

On the other hand, despite their high natural resource abundance, titanium alloys remain very expensive. This is mainly due to the high manufacturing cost of titanium alloys, which comes from the difficulties not only in the extraction of the metal, but also in the fabrication of the alloys from the respective metals. An example for the latter is the β-phase-enriched TiZrNbTa alloy with lower elastic modulus without compromising the biocompatibility. Unfortunately, making such $\alpha+\beta$ alloys is very expensive, because of the difficulties in using the high-temperature vacuum and in alloying Ta (Nb) with Ti(Zr), because of the large differences in density and melting point.[13,14]

Recently, a novel process, called the FFC Cambridge Process, has been reported for the preparation of titanium, silicon, zirconium, niobium, chromium, and their alloys via direct electrochemical reduction of solid oxides or mixed-oxide precursors in molten salts.[15−27] This new process is low in cost, simple in operation, and has the potential to replace the Kroll process, which is the conventional route for producing titanium and zirconium. As expected, pure titanium and zirconium that were produced by reducing their oxides in molten $CaCl_2$ were usually present in the α-phase.[26−29] Occasionally, β-phase titanium was found in the incompletely reduced TiO_2 pellet,[25] whereas, if a β-stabilizer was introduced, it was common to obtain β-phase titanium alloys, such as TiW or TiMo, through this electrolytic process.[22,23]

Most recently, we reported that well-sintered zirconium metal can be directly fabricated via the electrolysis of porous ZrO_2 pellets in molten $CaCl_2$ at 900 °C.[30] In this study, phase-tunable TiZr alloys in a consolidated porous structure, with elastic moduli of ~20−40 GPa, were prepared via the electrolysis of mixed TiO_2-ZrO_2 precursors. For the first time, we demonstrate that different phase combinations, namely, α-, $\alpha+\beta$-, and β-phases, can be realized in the TiZr alloys by simply controlling the trace oxygen content in the electrolysis products. The oxygen, as a sixpenny alloying element and usually being regarded as an α-phase stabilizer, acted as a phase-transition inhibitor to the transition from the high-temperature β-TiZr to the low-temperature α-TiZr. Furthermore, the physiochemical measurements confirmed the improved mechanical and anticorrosive performances of the as-electrolyzed β-phase-containing TiZr alloys, promising direct artificial implant applications.

2. Experimental Section

The equimolar mixture of TiO_2 (≥ 98.0%, Shanghai Pudong Chemical Reagent Company, PRC) and ZrO_2 powders (≥99.0%, Sinopharm Chemical Reagent Co. Ltd., PRC) was ball-milled with anhydrous alcohol for 10 h. The milled product was pressed at 10 MPa into cylindrical pellets (13 mm in diameter, 1.5−1.6 mm thick, mass of ca. 0.66 g) that were sintered at 300 °C for 2 h. The pellet was wrapped with molybdenum wires to form an assembled cathode and electrolyzed under constant voltage in molten $CaCl_2$ with a graphite rod anode. A sealable stainless steel tube reactor was used for electrolysis. Approximately 750 g of anhydrous $CaCl_2$ (≥96.0%, Shanghai Meixing Chemicals) were contained in a large graphite crucible, and dried in the reactor for more than 48 h at 200−300 °C in air. Subsequently, the reactor was sealed and continuously flushed with argon (>99.999%) when the temperature was increased to and maintained at 500−700 °C for 5 h, and finally increased to 900 °C. Pre-electrolysis was performed at 2.6 V between a nickel sheet cathode and the graphite rod anode for a sufficiently long time to further remove residual water and some redox active impurities from the molten salt. During electrolysis, the effluent gas from the reactor was guided into a buffering bottle filled with anhydrous $CaCl_2$ granules, a flask filled with concentrated H_2SO_4, and then through a solution of 0.1 M NaOH before escaping into a fume hood. The electrolysis was controlled by a high-accuracy four-electrode battery testing system (Shenzhen Neware Electronic Ltd., PRC) that was linked to a personal computer (PC).

Unless specified, the electrolyzed product was lifted into a cooling argon stream at ca. 500 °C for 10 min, then cooled in air to room temperature, washed in distilled water, and dried under vacuum. It was then examined by scanning electron microscopy (SEM) (FEI Sirion Field Emission Gun SEM), energy-dispersive X-ray spectroscopy (EDX) (EDAX GENESIS 7000), powder X-ray diffraction (XRD) (Shimadzu X-ray 6000 with Cu $K\alpha_1$ radiation at λ = 1.5405 Å), and inert-gas fusion-infrared absorption oxygen analysis (RO-416DR, LECO, USA). Microhardness test was performed on a Vickers microhardness tester (HXS-1000A, made in Shanghai, PRC). The three-point bending test was conducted on the Instron-type universal test machine (Instron 8841).

Corrosion behavior was studied in the simulated physiologic Ringer solution (8.61 g/L NaCl, 0.49 g/L $CaCl_2$, 0.30 g/L KCl) at 37 °C. The studied alloy was sealed by epoxy with an exposed working surface. Before immersion into the electrolyte, the working surface was sequentially ground on silicon carbide (SiC) paper up to grade 3000, followed by rinsing in deionized

(12) Ryan, G.; Pandit, A.; Apatsidis, D. P. *Biomaterials* **2006**, *27*, 2651.
(13) Niinomi, M. *Biomaterials* **2003**, *24*, 2673.
(14) Li, S. J.; Yang, R.; Niinomi, M.; Hao, Y. L.; Cui, Y. Y.; Guo, Z. X. *Mater. Sci. Technol.* **2005**, *21*, 678.
(15) Chen, G. Z.; Fray, D. J.; Farthing, T. W. *Nature* **2000**, *407*, 361.
(16) Nohira, T.; Yasuda, K.; Ito, Y. *Nat. Mater.* **2003**, *2*, 397.
(17) Jin, X. B.; Gao, P.; Wang, D. H.; Hu, X. H.; Chen, G. Z. *Angew. Chem. Int. Ed.* **2004**, *43*, 733.
(18) Wu, T.; Xiao, W.; Jin, X. B.; Liu, C.; Wang, D. H.; Chen, G. Z. *Phys Chem. Chem. Phys.* **2008**, *10*, 1809.
(19) Chen, G. Z.; Gordo, E.; Fray, D. *Metall. Mater. Trans. B* **2004**, *35*, 223.
(20) Yan, X. Y.; Fray, D. J. *Adv. Funct. Mater.* **2005**, *15*, 1757.
(21) Ma, M.; Wang, D. H.; Hu, X. H.; Jin, X. B.; Chen, G. Z. *Chem. Eur. J.* **2006**, *12*, 5075.
(22) Bhagat, R.; Jackson, M.; Inman, D.; Dashwood, R. *J. Electrochem. Soc.* **2008**, *155*, E63.
(23) Bhagat, R.; Jackson, M.; Inman, D.; Dashwood, R. *J. Electrochem. Soc.* **2009**, *156*, E1.
(24) Kar, P.; Evans, J. W. *Electrochem. Commun.* **2006**, *8*, 1397.
(25) Centeno-Sanchez, R. L.; Fray, D. J.; Chen, G. Z. *J. Mater. Sci.* **2007**, *42*, 7494.
(26) Ma, M.; Wang, D. H.; Wang, W. G.; Hu, X. H.; Jin, X. B.; Chen, G. Z. J. *Alloy. Compd.* **2006**, *420*, 37.
(27) Li, Q. Y.; Du, J. H.; Xi, Z. P. *Rare Met. Mater. Eng.* **2007**, *36* (Special Suppl. 3), 390.
(28) Park, I.; Abiko, T.; Okabe, T. H. *J. Phys. Chem. Solids* **2005**, *66*, 410.
(29) Okabe, T. H.; Oda, T.; Mitsuda, Y. *J. Alloy. Compd.* **2004**, *364*, 156.
(30) Peng, J. J.; Jiang, K.; Xiao, W.; Wang, D. H.; Jin, X. B.; Chen, G. Z. *Chem. Mater.* **2008**, *20*, 7274.

water. A saturated calomel electrode (SCE) and a platinum foil served as the reference and counter electrodes, respectively. Potentiodynamic polarization scans were conducted at a scan rate of 1 mV/s in the potential range from −0.8 V to 2.2 V (vs SCE). A Basic Electrochemical System (EG&G Instrument) was used for the measurement.

3. Results and Discussion

3.1. The Electrochemical Reduction of TiO_2−ZrO_2 Mixture in Molten $CaCl_2$. *3.1.1. Constant Voltage Electrolysis.* Constant voltage electrolysis was applied to reduce the pelletized TiO_2−ZrO_2 mixture (1:1 molar ratio, ca. 0.7 g in mass) with a graphite anode in molten $CaCl_2$ at 900 °C. The current−time (I−t) plot, as exemplified in Figure 1a, was recorded during the electrolysis at 3.0 V for 16 h. It shows an initial fast increase current to a peak (see the inset) in the first few minutes, which is followed by a quick decline in the next few minutes. In the remaining time, the current change is slower, going through multiple steps and then ends at the low level as the background current. This feature, according to the literature,[30−32] suggests that the process continued with the reduction of the oxide pellets occurring at the metal/oxide/electrolyte three-phase interlines (3PIs). The 3PIs expand along the pellet's surface first, leading to the current peak on the I−t plot, and then propagate into the pellet with a declining current tail at later times of the electrolysis due to the increasing ohmic drop and concentration polarization with the 3PIs penetrating deeper into the pellet.[31−33]

To identify the intermediate products during the constant voltage electrolysis at 3.0 V, an array of experiments with different electrolysis times were performed. The products were washed in water, dried, and analyzed via XRD, scanning electron microscopy (SEM), and energy-dispersive X-ray (EDX) spectroscopy. The electrolysis times were selected as follows: 15 min, then with every increment of 15 min to 1 h, followed by every hour until 16 h. Some typical XRD results are shown in Figure 1b. It can be seen that the initial cathodic product contained the perovskite phase and a small amount of TiO_x ($x < 2$), particularly, Ti_zO ($z = 2, 3, 6$). This initial product had an ash black color, differing from the precursor's white color. The perovskite phases may include $CaTiO_3$ and $CaZrO_3$, both of which have almost the same lattice parameters. These perovskite phases could have formed, either by the chemical reaction between the remaining oxide in the pellet and the electrochemically generated O^{2-} ions and the Ca^{2+} ions from the molten salt, or by the direct electrochemical inclusion of the Ca^{2+} into the parent oxide phase, which would be more likely for

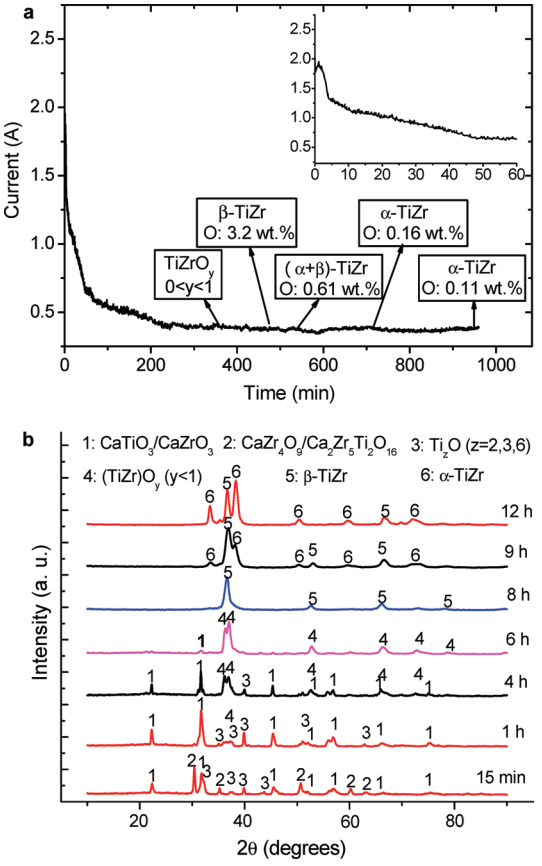

Figure 1. (a) Typical current−time plot recorded during constant voltage electrolysis of two TiO_2−ZrO_2 pellets (1.5−1.6 mm thick, ~13.0 mm in diameter, mass of ~0.66 g) in molten $CaCl_2$ at 3.0 V and 900 °C. (b) XRD patterns of the products from electrolysis at 3.0 V for different times, as indicated.

TiO_2.[30,34−36] It is worth mentioning that the Ca^{2+} and O^{2-} ions may take part directly in the perovskite formation or combine into the CaO precipitate at a relatively high electroreduction rate.[33] Note that the Ca, Zr, Ti, and O elements in the perovskite products, as revealed by EDX determination, are present in nonstoichiometric proportion, probably indicating the formation of the defective compounds such as $Ca_\delta Ti(Zr)O_\xi$ ($\delta \leq 1, \xi \leq 3$). Figure 1b also shows that the XRD patterns of these defective compounds show small but noticeable deviations in the diffraction angles from those of standard $CaTiO_3$ and $CaZrO_3$. These changes indicate lattice distortion and are in agreement with our previous studies.[30,34] The XRD patterns also present some other perovskite phases, such as $Ca_2Zr_5Ti_2O_{16}$ and $CaZr_4O_9$, which were likely formed through the chemical reactions between the oxide precursor and the CaO. With increasing electrolysis time, the perovskites previously mentioned were reduced to pseudo-oxides, namely, $(TiZr)O_y$ ($y < 1$), which can be derived from the O−Ti and O−Zr binary phase diagrams.

The gradual progress of the electroreduction of the oxide pellet can also be demonstrated by Figure 2a, which displays the cross section of the TiO_2−ZrO_2 pellet after 4 h of electrolysis at 3.0 V, showing the typical "sandwich"

(31) Xiao, W.; Jin, X. B.; Deng, Y.; Wang, D. H.; Chen, G. Z. *Chem. Eur. J.* **2007**, *13*(2), 604.
(32) Deng, Y.; Wang, D. H.; Xiao, W.; Jin, X. B.; Hu, X. H.; Chen, G. Z. *J. Phys. Chem. B* **2005**, *109*, 14043.
(33) Xiao, W.; Jin, X. B.; Deng, Y.; Wang, D. H.; Hu, X. H.; Chen, G. Z. *ChemPhysChem* **2006**, *7*, 1750.
(34) Jiang, K.; Hu, X. H.; Ma, M.; Wang, D. H.; Qiu, G. H.; Jin, X. B.; Chen, G. Z. *Angew. Chem. Int. Edit.* **2006**, *45*, 428.
(35) Dring, K.; Dashwood, R.; Inman, D. *J. Electrochem. Soc.* **2005**, *152*, E104.
(36) Abdelkader, A. M.; Daher, A.; Abdelkareem, R. A.; El-Kashif, E. *Metall. Mater. Trans. B* **2007**, *38*, 35.

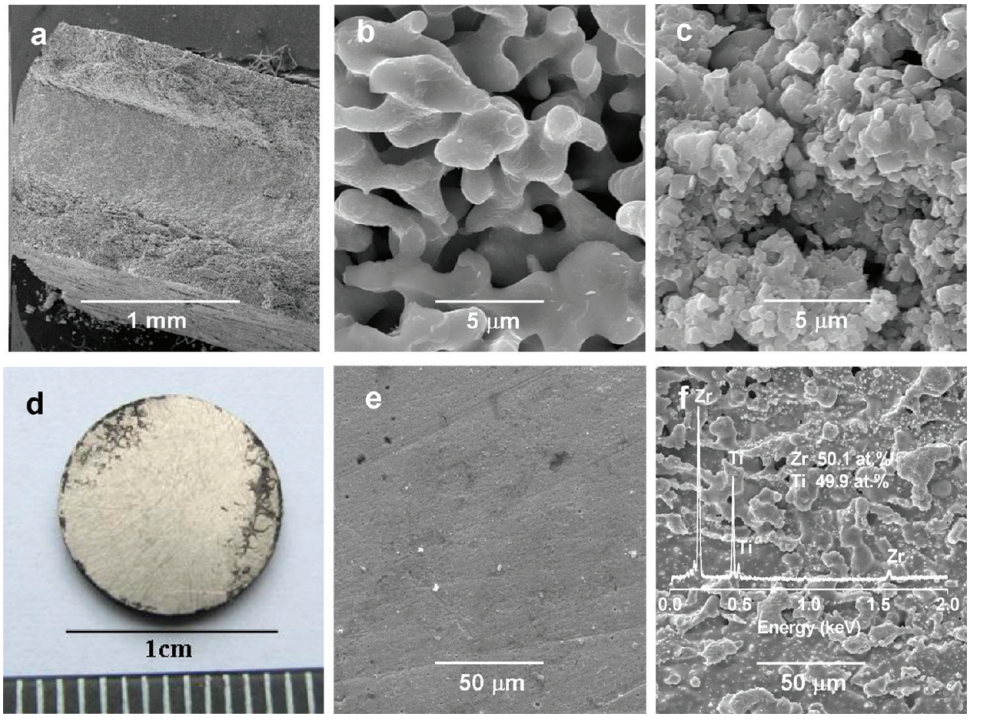

Figure 2. SEM images of (a) the cross sections of TiO_2-ZrO_2 pellet electrolyzed in molten $CaCl_2$ at 900 °C and 3.0 V for 4 h, (b) the outer layer shown in panel a, and (c) the inner layer of the sample in panel a at a higher magnification. (d) Digital photo of the ground pellet after electrolysis in molten $CaCl_2$ at 900 °C and 3.0 V for 12 h. SEM images of the ground surface and the cross section of the pellet in panel d are shown in panels e and f, respectively. The EDX spectrum shown in panel f was taken over the area of the image shown in panel f.

structure. As depicted, the electroreduction of the oxide pellet proceeded inward from the pellet's surface.[33,34] The outer layer of the pellet in Figure 2a at higher magnification is shown in Figure 2b, which looks like the pure metal with interconnected nodular particles similar to the electrochemically generated titanium metal from solid TiO_2.[15,34] These nodules were identified to be the pseudo-oxide, $(TiZr)O_y$, by both XRD and EDX analyses. The inner layer was composed of dense aggregates of irregular particles (see Figure 2c), which were identified to be mainly perovskites. The perovskite layer was completely reduced after about 6−7 h of electrolysis at 3.0 V, and the cross section of the cathode pellet changed from the "sandwich" structure to a uniform morphology, similar to that in Figure 2b. Subsequently, the O atom in the $(TiZr)O_y$ was ionized into the electrolyte, leading to the formation of the β-TiZr solid solution with the O atom as the solute in the 8 h of electrolysis. As illustrated in Figure 1, the electrolysis at longer times contributed to the electrodeoxygenation of the metal−oxygen solid solution. As exemplified in Figures 2d−f, the collected products were fully metallized into well-consolidated porous structures whose XRD patterns in Figure 1b confirmed the presence of either ($\alpha+\beta$)-TiZr or α-TiZr phases.

3.1.2. The Reduction Mechanism. According to the aforementioned discussion, the reduction mechanism of the TiO_2-ZrO_2 mixture electrode is schematically proposed in Scheme 1. The TiO_2-ZrO_2 mixture, particularly TiO_2, can be initially reduced either to $Ca_\delta Ti(Zr)O_\xi$ by the inclusion of the Ca^{2+} into the TiO_2 or to TiO_x with O^{2-} being released into the electrolyte. The electroreduction

Scheme 1. Schematic Representation of Mechanism for the Electroreduction of Mixed TiO_2-ZrO_2 (1:1 Molar Ratio) in Molten $CaCl_2$ at 900 °C

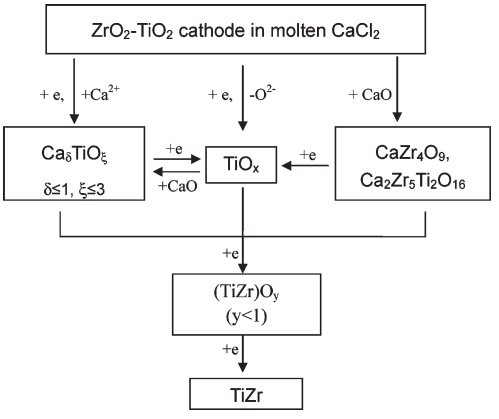

generated O^{2-} ions together with the Ca^{2+} ions from the molten $CaCl_2$ react chemically or electrochemically with ZrO_2, TiO_2, or TiO_x to form various perovskites. These perovskites, together with TiO_x, will be reduced to $(TiZr)O_y$ and finally to the TiZr alloy in either or both of the α and β structures.

3.2. Electrochemical Tuning of the Phases in the Electrolytic TiZr Alloys. We would like to highlight the experimental findings as shown in Figure 1b that, via the electroreduction method, α-TiZr, β-TiZr, and ($\alpha+\beta$)-TiZr alloys can be selectively obtained by simply controlling the electrolysis time. This finding is the first example showing that, without using any β-phase stabilizers, the electroreduction process has the capability to tune titanium alloys between the α-phase and β-phase. The collected

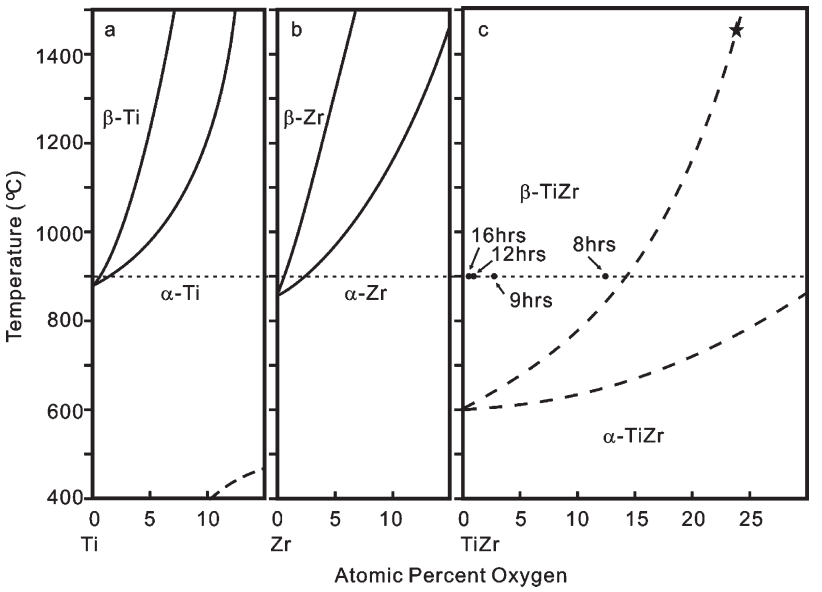

Figure 3. Binary phase diagrams of (a) O−Ti and (b) O−Zr. (c) Schematic approximation of the TiZr−O binary phase diagram derived from the Ti−Zr binary phase diagram and the Ti−Zr−O ternary phase diagram at 1450 °C (represented by the star, ★),[37] with some data extracted from Figure 2a.

product from the 8 h of electrolysis was mainly β-TiZr, while the α-phase could be found in the 9-h product. The α-phase in the (α+β)-TiZr increased as the electrolysis time increased until to 12 h, then the β-phase disappeared and the collected product became dominated by α-TiZr.

Generally, in the electroreduction process, the electrolysis time can be related to the content of oxygen remaining in the generated metal. Usually, the longer the electrolysis time, the lower the oxygen content, which is obviously true in this study, as indicated in Figure 1a. The oxygen content in the β-TiZr formed in the 8 h of electrolysis was ∼3.2 wt %, and decreased to ∼0.61 wt % in the (α+β)-TiZr and 0.16 wt % in the α-TiZr formed after electrolysis for 9 h and 12 h, respectively. The sample that was electrolyzed for 16 h contained only 0.11 wt % (= 1100 ppm) oxygen. Thus, it is important to reveal the effect of the oxygen content on the crystal structure in the final collected alloy. Oxygen is often regarded as an element capable of stabilizing the α-structure of titanium and zirconium, which is in accordance with the O−Ti or O−Zr binary phase diagrams. As can be seen in Figure 3, at 900 °C, α-Ti or α-Zr would exist over a large range of oxygen content while β-Ti and β-Zr would not form if the oxygen contents are higher than 0.4 wt % and 0.3 wt % in Ti and Zr, respectively. The O−TiZr binary phase diagram is not available in the literature, but it is expected to have similar features as the O−Ti and O−Zr phase diagrams. Thus, by analyzing the O−Ti and O−Zr binary constant pressure phase diagrams and the Ti−Zr−O ternary phase diagram at 1450 °C,[37] a schematic was constructed to approximate the TiZr−O binary phase diagram in Figure 3c with some experimental data added to help the discussion. Clearly, at 900 °C, the thermodynamically stable phase of the TiZr should be the α-phase with a higher oxygen content, but instead, it is the β-phase with a lower oxygen content, which is, however, opposite to our experimental findings on the collected products, as indicated in Figure 1.

Considering that only α-TiZr is stable thermodynamically at room temperature, the collected β-phase TiZr products in this study could only be metastable and should have formed at 900 °C during the electrolysis. According to the schematic O−TiZr binary phase diagram in Figure 3c, the fact that the collected product with 3.2 wt % oxygen at room temperature was dominated by the β-phase indicates that all the as-electrolyzed alloys from longer electrolysis times, as shown in Figure 1a, should be in the β-phase at 900 °C. During cooling to room temperature, the β-to-α phase transition would occur; however, it seems that the transformation rate was highly dependent on the oxygen content in the alloy. The higher was oxygen content, the slower the transition rate, leading to either or both of α- and β-phases in the TiZr products. In other words, the phases or crystal structures of the TiZr alloys are tunable by controlling the oxygen content in the alloys. Oxygen, on the other hand, can be regarded as an inhibitor to the phase transformation of TiZr, as being revealed by some earlier studies on some other titanium alloys.[38,39] The phase-transition rate of pure or low-oxygen TiZr should be very quick, as can be derived from the fact that there is no report in the literature on the observation of β- or (α+β)-phases in the TiZr products from the traditional smelting process from individual Ti and Zr, in which β-TiZr must have formed at high temperatures. In this study, it was found that, with a lower oxygen content, the TiZr products, such as those collected after 16 h of electrolysis at 3.0 V, were all in the α-phase, even if they were quenched directly from 900 °C in cold water. However, if the oxygen

(37) Lin, K. L.; Lin, C. C. *J. Am. Ceram. Soc.* **2007**, *90*, 893.

(38) Lin, K. L.; Lin, C. C. *J. Am. Ceram. Soc.* **2005**, *88*, 1268.
(39) Huang, A.; Loretto, M. H.; Hu, D.; Liu, K.; Wu, X. H. *Intermetallics* **2006**, *14*, 838.

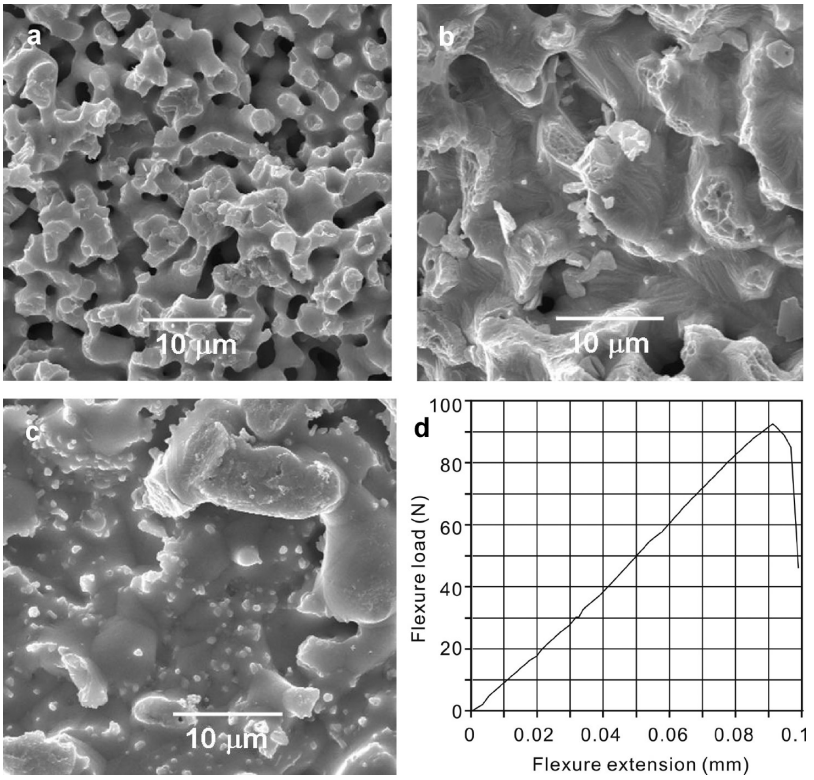

Figure 4. SEM images of the as-produced TiZr alloys from electrolysis in molten $CaCl_2$ at 900 °C: (a) β-TiZr, 3.0 V, 8 h; (b) (α+β)-TiZr, 3.1 V, 6 h; and (c) α-TiZr, 3.0 V, 12 h. (d) Load−extension curve from the three-point bending test of sample 1, as listed in Table 1.

content increased, it was quite easy to determine the β-phase in the final product, although the proportion of the β-phase was dependent on the quenching condition.

Linking to Figure 3c, the role of oxygen should be two-fold in influencing the crystal structures of the TiZr alloy. Taking 900 °C as an example, if the oxygen content is higher than a certain critical value, only α-TiZr can form at 900 °C, and it is impossible to obtain any β-TiZr in the final product. In such cases, oxygen can be regarded as a α-stabilizer to influence the crystal structure. However, once the oxygen content declines to allow the formation of pure β-TiZr, the oxygen solute becomes an inhibitor to the β-to-α phase transformation of TiZr during cooling. Obviously, this inhibitor effect of oxygen disappears when the oxygen content becomes too low. In other words, there exists a medium range of oxygen content that is beneficial to the formation of the metastable β-TiZr at room temperature. Thus, the electrolysis process can tune between the α- and β-phases in the produced TiZr alloy by simply controlling the electrolysis time and, hence, the oxygen content that remains in the alloy.

3.3. Physiochemical Measurements of the Electrolytic TiZr Alloys. Similar to the consolidated zirconium metal generated via in situ sintering during the electrolysis of porous ZrO_2 pellets,[30] the as-electrolyzed TiZr alloys were also found to be in the consolidated porous structure, as shown in Figures 2d−f. Here, the microstructures of the TiZrs with different phase components were further examined via SEM (see Figures 4a−c). It can be seen that the metal particles in all the samples sintered together. There are some apparent pores in the β-TiZr (see Figure 4a), but the (α+β)-TiZr (see Figure 4b) and α-TiZr (see Figure 4c) sintered to almost dense morphologies, which would have ensured enough strength to be directly used as devices without the need for any further physical process (for example, smelting or pressing). The porosities of both (α+β)-TiZr and α-TiZr were ~25%, as estimated by comparing the theoretically calculated density of the TiZr alloy and the weight/volume ratios of the as-electrolyzed pellets. As it was reviewed in the Introduction section, the introduction of the β-phase into the TiZr alloy would result in a decrease in the elastic modulus and improvement of the anticorrosive performance of the alloy as required for a biomaterial, whilst the inherent porosity in the as-electrolysed pellet would reduce the elastic modulus further. To evaluate the possibility of the electrolytic TiZr alloys for medical implant applications, some physiochemical measurements were carried out and discussed below.

3.3.1. Bending Strength and Elastic Modulus. As mentioned previously, the as-produced electrolytic TiZr alloys were strong enough for some strength tests. As demonstrated in Figure 2d, the as-electrolyzed pellets were round in shape, ~11 mm in diameter and 1 mm thick, which were ground to a rectangular shape (~10 mm × ~5 mm) for the three-point bending tests. The β-TiZr sample with large numbers of pores was determined to be too brittle. Thus, only the (α+β)-TiZr and α-TiZr samples were randomly selected and tested. One of the obtained load-extension curves is presented in Figure 4d. Typically, there was a linear relationship between the flexure load and the flexure extension,

Table 1. Bending Strengths and Elastic Moduli of As-Produced Electrolytic TiZr Pellets

sample	phase structure	electrolysis conditions	bending strength (MPa)	elastic modulus (GPa)
1	(α+β)-TiZr	3.0−3.1 V, 8−10 h	309	25
2	(α+β)-TiZr	3.0−3.1 V, 8−10 h	263	24
3	α-TiZr	3.0−3.1 V, 11−13 h	567	40
4	α-TiZr	3.0−3.1 V, 11−13 h	606	37

relative to the elastic deformation, followed by fracture of the sample as the maximum load was reached. The bending strength and elastic modulus of each sample listed in Table 1 were calculated from the slope and the geometric dimensions of the samples.

Table 1 shows that the elastic modulus of the as-produced α-TiZr sample (~40 GPa) is significantly lower than that of arc-smelting cast TiZr (~100 GPa), but much closer to that of natural bone (10−30 GPa), which could have possibly resulted from the porous structure in the as-electrolyzed pellet. The (α+β)-TiZr pellet with an elastic modulus of ~25 GPa, which shows an additional 40% decrease from that of the α-TiZr pellet, is more favorable for the medical implant applications, in terms of mechanical matching. On the other hand, the bending strength of the α-TiZr pellet is greater than that of the (α+β)-TiZr, which is very much comparable to that of commercially pure titanium (CP-Ti).[9] However, both the bending strengths of the α-TiZr and the (α+β)-TiZr pellets are much greater than that of natural bone.[11]

3.3.2. Microhardness. Figure 5a shows the microhardness data of some samples electrolyzed at 3.0 V and 900 °C for different times. The Vickers hardness of the smelting-cast dense α-TiZr was reported to be ~350, which is almost twice as large as that of CP-Ti.[9,40] In this study, the hardness of the α-TiZr pellets obtained from 12 h and 16 h of electrolysis were only ~150. Note that the as-electrolyzed pellets were all porous, which would lead to smaller hardness values. However, the formation of the β-phase also could have contributed to increasing the hardness of the electrolyzed product. As shown in Figure 5a, the microhardness of the as-produced TiZr pellet increased as the electrolysis time decreased (or as the β-phase proportion increased), which is in agreement with the general rule on titanium alloys.[1] As indicated in Figure 5b, plotting the hardness against the square root of the oxygen content can also lead to a straight line, which is in accordance with the known empirical linear relationship between the two variables.[8,41] For the as-produced α-TiZrs to (α+β)-TiZr, there is a very large increase (30%−50%) in hardness, which may benefit by improving the wear resistance of the electrolytic products.

3.3.3. Corrosion Behavior. Except for the pellet electrolyzed for 8 h, all the samples, as studied in Figure 5, and a CP-Ti sample were ground and polished to a mirror

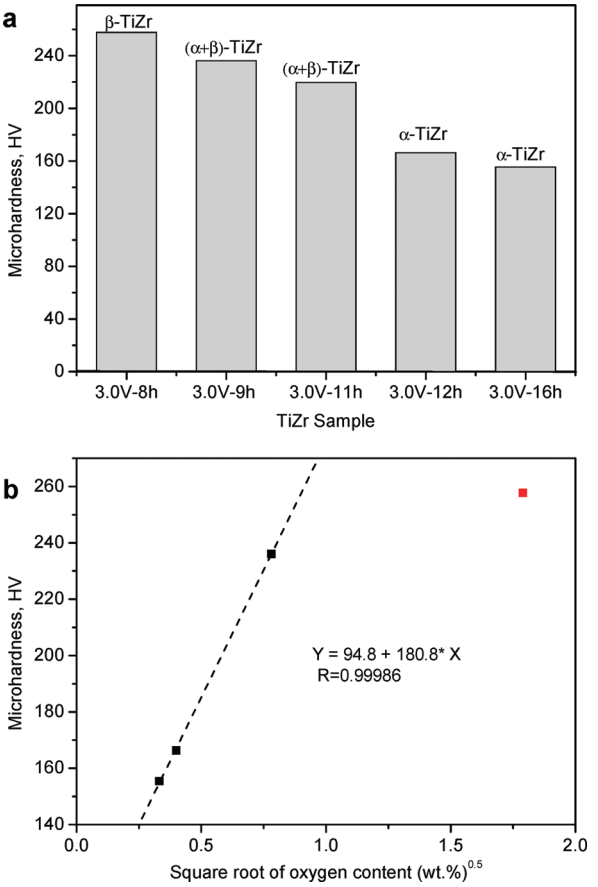

Figure 5. (a) Microhardness of the as-produced TiZr alloys (with their crystal structures indicated) from electrolysis in molten $CaCl_2$ at 3.0 V for different times. (b) Plots of the hardness of the electrolytic TiZr against the square root of the oxygen content.

finish, and were studied for their corrosion resistance in the Ringer solution by electrochemical means. Figure 6 shows some typical experimental results. As presented in Figure 6a, during the open circuit potential (OCP) measurement, the OCP of each sample slowly shifted to a reasonably stable less negative potential, indicating the spontaneous passivation of the metal in the Ringer solution, because of the formation of surface oxide layer. It can be seen that the 3.0 V−9 h electrolytic (α+β)-TiZr presents the least negative corrosion potential (E_{corr}) of approximately −67 mV (vs SCE), whereas those of the 3.0 V−12 h α-TiZr and the CP-Ti are both approximately −170 mV (vs SCE). Figure 6b displays the corresponding polarization curves. Again, the (α+β)-TiZr shows the most positive corrosion potential (−230 mV (vs SCE)) and the lowest corrosion current (I_{corr} = 0.105 μA/cm^2). The corrosion potentials determined from the polarization curves are more negative than those obtained from the OCP measurements, which are similar to the literature reports and were usually explained by the removal of the original oxide layer on the metal under the highly reducing initial potential (−800 mV (vs SCE)) used in the measurement.[42,43] Note that the porous structure of the

(40) Kobayashi, E.; Matsumoto, S.; Doi, H.; Yoneyama, T.; Hamanaka, H. J. *Biomed. Mater. Res* **1995**, *29*, 943.
(41) Chan, K. S.; Koike, M.; Johnson, B. W.; Okabe, T. *Metall. Mater. Trans. A* **2008**, *39A*, 171.
(42) Cai, Z.; Shafer, T.; Watanabe, I.; Nunn, ME.; Okabe, T. *Biomaterials* **2003**, *24*, 213.
(43) Oliveira, N. T. C.; Ferreira, E. A.; Duarte, L.; Biaggio, S. R.; Rocha-Filho, R. C.; Bocchi, N. *Electrochim. Acta* **2006**, *51*, 2068.

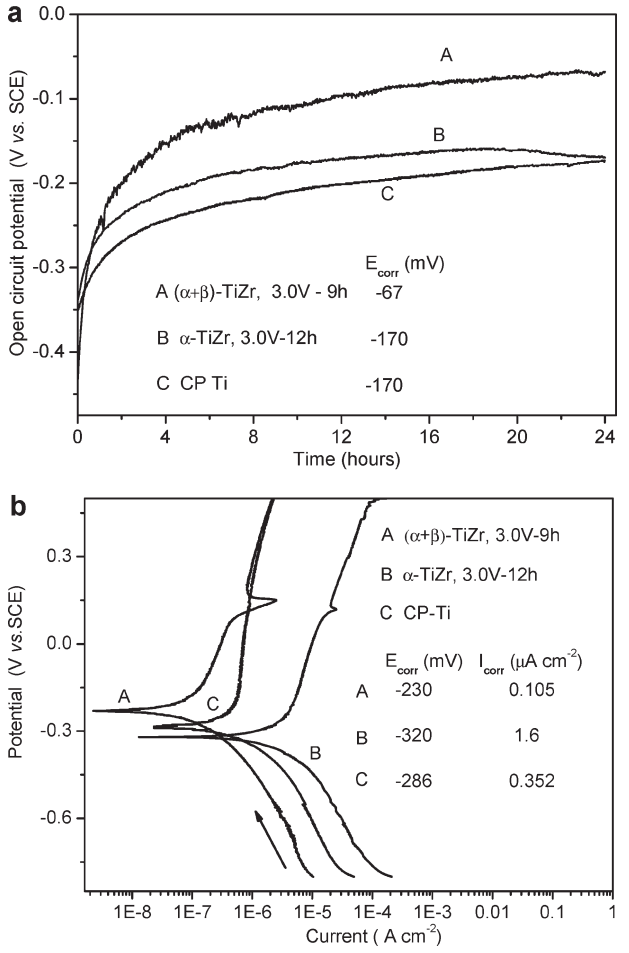

Figure 6. (a) Plots of the open circuit potential (OCP) against the standing time for the as-produced TiZr alloys and the CP-Ti in the Ringer solution at 37 °C. (b) Polarization curves of the samples described in panel (a) after 24 h of immersion in the Ringer solution at 37 °C. Scan rate: 1 mV/s. The respective corrosion potential (E_{corr}) and the corrosion current (I_{corr}) evaluated from each measurement are listed.

as-electrolyzed pellets would have led to a negative corrosion potential and larger corrosion current. However, both electrochemical measurements indicate improved anticorrosive performance of the as-produced electrolytic (α+β)-TiZr, in comparison with the α-TiZr and the dense CP-Ti.

4. Limit of Deoxygenation

The findings and discussion presented in the previous sections highlight the important influence of the oxygen content on the properties of the TiZr alloys produced by direct electroreduction of the oxide precursors. It was reported that,[44−46] consistent with thermodynamic analyses, titanium wires or foils 1−2 mm thick could be cathodically deoxygenated in molten $CaCl_2$ within several hours. The oxygen content was claimed to be 10−200 ppm, which is much lower than that reported in Figure 1b for the TiZr alloys, although the electrolysis was performed under comparable conditions for a longer time. Similar findings were reported for other metals, such as titanium and niobium, as well as zirconium, and their alloys from electroreduction of the respective oxide precursors,[15,18−30,47] which warrants further discussion.

Both titanium and zirconium have high corrosion resistivity, because of a dense oxide layer a few nanometers thick that forms spontaneously on the surface of the metal that is in contact with air, even at room temperature. This oxide layer has negligible influence on the properties of bulk solid samples, such as the thin wires or foils, but can be a significant origin of oxygen in powdery or porous metals. For example, assuming a 3-nm-thick oxide layer, the oxygen contents in spherical titanium particles 0.5 and 5.0 μm in diameter are 14500 ppm and 1500 ppm, respectively. Considering that the Ti−Zr alloys also have high oxygen solubility in the solid state, the oxygen contents reported in Figure 1b agree fairly well with the morphologies revealed by the SEM images in Figures 2 and 4, according to the attribution of the surface oxide layer. In fact, transmission electron microscopy (TEM) has offered direct evidence for the presence of uniform nanometer-thick oxide coatings on individual particles of the tantalum and niobium powders, as produced by the electroreduction method.[18,47] Thus, unless the contact with air (or water) is avoided, the powdery or porous Ti−Zr alloys from electroreduction of the oxide precursors would have a lower limit of oxygen content determined largely by the specific surface area of the products.

5. Conclusions

In conclusion, (α+β)-TiZr alloys with a tunable β-phase proportion were prepared by direct electrolysis of solid TiO_2 and ZrO_2 mixture in molten $CaCl_2$ at 900 °C. First, the mixed-oxide precursor is reduced to $Ca_\delta Ti(Zr)O_\xi$ ($\delta \leq 1$, $\xi \leq 3$) and TiO_x ($x < 2$) with some complicated perovskite phases, such as $Ca_2Zr_5Ti_2O_{16}$ and $CaZr_4O_9$, formed simultaneously by chemical reactions between the CaO and the TiO_2, ZrO_2, or TiO_x. The intermediates are then reduced together to $(TiZr)O_y$ ($y < 1$) and finally to the TiZr alloy. The tuning of the proportion of the α- and β-phases in the electrolytic TiZr alloys can be readily achieved by controlling the oxygen content in the alloys. The trace oxygen in the product with its content determined by the electrolysis time under certain conditions might have served as an inhibitor to the phase transition from the high-temperature β-TiZr to the low-temperature α-TiZr, leading to metastable β-TiZr in the final product at room temperature. While the oxygen content decreased to < 1100 ppm, only α-TiZr was collected.

The as-produced (α+β)-TiZr and α-TiZr were in well-consolidated porous structures with porosities of ~25%. They were comparable to natural bone in elastic modulus, particularly, the elastic modulus of the (α+β)-TiZr

(44) Okabe, T. H.; Nakamura, M.; Oishi, T.; Ono, K. *Metall. Trans. B* **1993**, *24*, 449.
(45) Chen, G. Z.; Fray, D. J.; Farthing, T. W. *Metall. Trans. B* **2001**, *32*, 1041.
(46) Ono, K.; Suzuki, R. O. *JOM* **2002**, *54*, 59.
(47) Wu, T.; Jin, X. B.; Xiao, W.; Hu, X. H.; Wang, D. H.; Chen, G. Z. *Chem. Mater.* **2007**, *19*, 153.

(25 GPa) fell within the range of that of natural bone. The α-TiZr had higher strength, while the (α+β)-TiZr possessed greater microhardness and enhanced corrosion resistance.

Note that, using this simple electrochemical method, β-phase and (α+β)-phase TiZr alloys can be readily produced without the addition of any bio-incompatible β-phase stabilizing elements and/or any other expensive element such as tantalum. This advantage of the electroreduction method is demonstrated for the first time and, together with the other merits of this novel process, promises a new route for the production of better and more affordable TiZr alloys for biomedical applications. In addition, if the oxide precursor is made in the correct shape and dimensions,[30] the well-consolidated as-produced Ti−Zr alloys may be directly machined into, for example, a dental implant without the need for any treatment at elevated temperatures. It may also be possibile to apply the as-produced porous or powdery Ti−Zr alloys in the cold-press molding process for the manufacturing of more-complicated artifacts. We believe the findings presented in this paper and the technological prospects can also lead to a generic approach for other titanium alloys, either powder or artifacts, with tunable crystal structures and, hence, the desired material properties.

Acknowledgment. The authors acknowledge the financial support from the NSFC (Nos. 20773094 and 20403012), the National Key Fundamental R&D Program of China (No. 2007CB613801), and the EPSRC (EP/F026412/1).